Selective Water Pore Recognition and Transport through Self-Assembled Alkyl-Ureido-Trianglamine Artificial Water Channels

Iuliana M Andrei, Arnaud Chaix, Belkacem Tarek Benkhaled, Romain Dupuis, Chaimaa Gomri, Eddy Petit, Maurizio Polentarutti, Arie van der Lee, Mona Semsarilar, Mihail Barboiu

Selective Water Pore Recognition and Transport through Self-Assembled Alkyl-Ureido-Trianglamine Artificial Water Channels

Iuliana M. Andrei,[‖] Arnaud Chaix,[‖] Belkacem Tarek Benkhaled, Romain Dupuis, Chaimaa Gomri, Eddy Petit, Maurizio Polentarutti, Arie van der Lee, Mona Semsarilar,* and Mihail Barboiu*

ABSTRACT: In nature, aquaporins (AQPs) are proteins known for fast water transport through the membrane of living cells. Artificial water channels (AWCs) synthetic counterparts with intrinsic water permeability have been developed with the hope of mimicking the performances and the natural functions of AQPs. Highly selective AWCs are needed, and the design of selectivity filters for water is of tremendous importance. Herein, we report the use of self-assembled trianglamine macrocycles acting as AWCs in lipid bilayer membranes that are able to transport water with steric restriction along biomimetic H-bonding-decorated pores conferring selective binding filters for water. Trianglamine [(±)**Δ**, (mixture of diastereoisomers) and $(R,R)_3$**Δ** and $(S,S)_3$**Δ**], trianglamine hydrochloride (**Δ.HCl**), and alkyl-ureido trianglamines (n = 4, 6, 8, and 12) [(±)**ΔC4**, (±)**ΔC8**, (±)**ΔC6**, and (±)**ΔC12**] were synthesized for the studies presented here. The single-crystal X-ray structures confirmed that trianglamines form a tubular superstructure in the solid state. The water translocation is controlled via successive selective H-bonding pores (a diameter of 3 Å) and highly permeable hydrophobic vestibules (a diameter of 5 Å). The self-assembled alkyl-ureido-trianglamines achieve a single-channel permeability of 10^8 water molecules/second/channel, which is within 1 order of magnitude lower than AQPs with good ability to sterically reject ions and preventing the proton transport. Trianglamines present potential for engineering membranes for water purification and separation technologies.

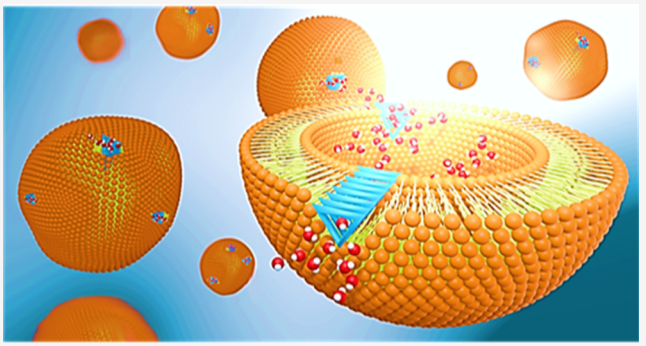

INTRODUCTION

In the very near future, the world will face a global water depletion and the forecasts are increasingly alarming. Nowadays, 4 billion people suffer from a lack of access to clean water, a number that could reach 5.7 billion in 2050 according to the United Nations' report.[1,2] Moreover, climate change, population growth, and the increase of industrial demand are accelerating the water scarcity. In order to counteract such factors and meet the needs of the population, innovative solutions are being researched within water purifications technologies. The past decade has seen the development of advanced membranes for the reverse osmosis (RO) as a major process for the production of millions of m^3 of desalinated water per day from oceans. Furthermore, a biomimetic approach to nature's functions in producing energy-efficient desalination membranes looking at artificial water channel (AWC)-based technologies appears as one of the solutions for low-energy water production. Nature has shown humankind its prowess; the goal would be to draw inspiration from the natural elements and design innovative, efficient, and less expensive technologies for water desalination. Aquaporins (AQPs) make up a family of protein-based membrane channels that play a crucial role in regulating the cellular osmotic pressure. AQPs efficiently conduct water across membrane bilayer while simultaneously exclude both hydrated ions (salts) and protons.[3−5] With very high selectivity and high rates of water transport (~10^9 H_2O molecules/s/channel),[6] AQPs have attracted interest in both academia and industries. Various attempts have been used to insert them into artificial membranes for water purification including medical and desalination applications.[7,8] However, manufacturing AQP-based membranes can be quite challenging because of their low stability to harsh pressure and salinity conditions as used in desalination. Bioinspired AWCs have been developed as an alternative strategy to overcome the limitations when using natural AQPs.[9] On the other hand, AWCs address effective advantages due to a lower cost of production, high tunability, stability, and membrane compatibility, as well as high pore packing density with the surface membrane permeability.[10,11]

Interestingly, recent studies report the successful integration of AWCs into polyamide RO membranes, confirming the promising approach for highly efficient biomimetic membranes for water desalination.[12]

In 2011, a series of pioneering work published by our group lead to the discovery of efficient AWCs such as I-quartet.[9,12−14] Since this discovery, several studies reported the construction of new classes of AWCs such as carbon nanotube porins (CNTPs),[15] aquafoldamers,[16] pillararenes (PAs),[17−20] peptide-appended Pillar[4]arenes (PAH[4]),[21] porous organic cages (POCs),[22] and hydroxy channels (octyl-ureido-polyols)[11,23] and more recently were reported fluorous oligoamide nanorings.[24]

Among these AWCs, few channels are able to translocate water with total salt rejection and the water vs ion/proton selectivity remains the actual challenge in creating novel designs.[25] As an example, CNTPs with the highest water transport (six times the AQPs) have one of the lowest selectivities.[15] For this purpose, there is a high demand in searching for new AWCs and synthetic macrocycles appear to be one of the promising approaches due to their intrinsic porosity and multiple possibilities to generate nanochannels via self-assembly. Several types of synthetic macrocycles,[26] such as crown ethers,[27] calixarenes,[28] cucurbituril,[29] pillararenes,[30] and many others,[31−34] have been designed for the development of applications such as separation, adsorption, catalysis, sensors, and drug delivery. Macrocycles can self-assemble through noncovalent interactions resulting in the formation of non-porous[35,36] or porous supramolecular organic frameworks with linear, layered, or interconnected channels.[37−40] Trianglamine macrocycles present several advantages due to their easy fabrication, purification, and scale-up at relatively low cost, making them an outstanding candidate so far for the construction of artificial aquaporins. Besides and since a recent decade, trianglamines have been used for several applications including gas capture/separation,[40] sensors,[41] membrane,[42] and host−guest chemistry.[43−45] To the best of our knowledge, no investigation was reported on the use of trianglamines as artificial aquaporins, emphasizing the novelty of this study.

Herein, we report the reference trianglamine (±)**Δ** (mixture of diastereoisomers),[46] (R,R)$_3$**Δ** and (S,S)$_3$**Δ**,[47] and trianglamine hydrochloride (**Δ.HCl**)[40] previously reported macrocycles together with the novel alkyl-ureido-trianglamines porins [(±)**ΔC4**, (±)**ΔC6**, (±)**ΔC8**, and (±)**ΔC12**] (mixture of diastereoisomers) (Scheme 1), which were selected for transport studies as selective water channels through lipid bilayer membranes.

The alkyl-ureido-trianglamine channels present unprecedented well-established water H-bonding pores with a diameter of ∼3 Å (pore size of aquaporins) which is considered as an ideal size to selectively bind water and sterically reject bigger hydrated ions, successively superposed with an intrinsic porosity of ∼5 Å diameter that fastly translocate water. The successive distribution H-bonding and hydrophobic regions displays noncontinuous waters within trianglamine channels, allowing high water transport with ion/proton rejection, making it a promising AWC platform.

RESULTS AND DISCUSSION

Design Strategy. The trianglamine (±)**Δ**, (R,R)$_3$**Δ**, (S,S)$_3$**Δ**, and trianglamine hydrochloride [(±)Δ.HCl] macrocycles were prepared as previously reported[40] by reacting (±)-trans-1,2-diaminocyclohexane or (R,R)*trans*-1,2 diaminocyclohexane or (S,S)*trans*-1,2 diaminocyclohexane (20 mmol) and terephthalaldehyde (20 mmol) in methanol in the presence of triethylamine (50 mmol), followed by reduction with sodium borohydride (3h) to afford (±)**Δ** consisting of a mixture of diastereomers composed of (R,R)$_3$**Δ**, (R,R)$_2$(S,S)**Δ**, (R,R)(S,S)$_2$**Δ**, and (S,S)$_3$ **Δ** trianglamines and (R,R)$_3$**Δ** and (S,S)$_3$**Δ** trianglamines, respectively (Figure S1).

Scheme 1. Chemical Structures of (±)Δ, (±)ΔC4, (±)ΔC6, (±)ΔC8, and (±)ΔC12

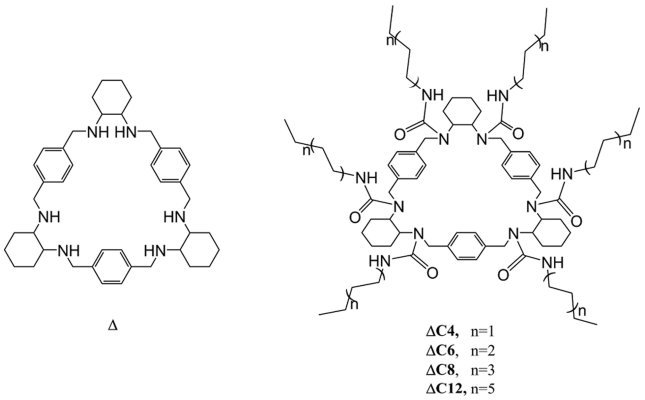

^{1}H and ^{13}C NMR spectra in $CDCl_3$ confirm the chemical structure of the macrocycles (±)**Δ**, (R,R)$_3$**Δ**, and (S,S)$_3$**Δ** (Figures S3−S8). High-resolution mass spectrometry (ESI-MS +) and high-resolution elemental analysis were in agreement with the proposed formula (Figures S9−S14). Thermogravimetric analysis (TGA) confirms that trianglamine **Δ** starts to decompose at 350 °C with a complete degradation at 400 °C (Figure S15). Furthermore, differential scanning calorimetry (DSC) of the trianglamine (±)**Δ** showed crystallization and melting temperatures of 45 and 150 °C, respectively (Figure S16). We then synthesized four new lipophilic trianglamines in order to increase their solubility, insertion, and stabilization into the lipid bilayer membranes. The (±)**ΔC4**, (±)**ΔC6**, (±)**ΔC8**, and (±)**ΔC12** were prepared through a one-step reaction in dry dichloromethane between the butyl-isocyanate **C4**, hexyl-isocyanate **C6**, octyl-isocyanate **C8**, and dodecyl-isocyanate **C12**, respectively, and the six secondary amines of the trianglamine, (±)**Δ** (Scheme 1). The obtained alkyl-ureido-trianglamines were washed with hexane using centrifugation and without the need for further purification (yield ∼95%) (Figure S2). Based on water permeation results (see below the Water Transport Experiments) showing similar performances for racemic and enantiomeric trianglamines, we decided to use the racemic (±)**Δ** inside (R,R)$_3$**Δ** and (S,S)$_3$**Δ** enantiomers as a starting reagent for the synthesis of the hydrophobic (±)**ΔCX** compounds. Moreover, this is beneficial enough to produce at high scale and at lower cost stable active trianglamines for membrane engineering for water purification.

^{1}H and ^{13}C NMR, ESI-MS, high-resolution elemental analysis, Fourier-transform infrared (FTIR), and TGA confirmed the successful functionalization of the trianglamine with alkyl-ureido-chains. Interestingly, the ^{1}H NMR spectra of the alkyl-ureido-trianglamines (±)**ΔC4**, (±)**ΔC6**, (±)**ΔC8**, and (±)**ΔC12** performed in $CDCl_3$ showed broad signals, most probably due to the formation of highly self-aggregated oligomers fastly self-exchanging in solution (Figures S18−S21). In dimethyl sulfoxide (DMSO) and upon heating at 100 °C (Figures S22−S25), the ^{1}H NMR signals of the alkyl-ureido-trianglamines (±)**ΔC4**, (±)**ΔC6**, (±)**ΔC8**, and

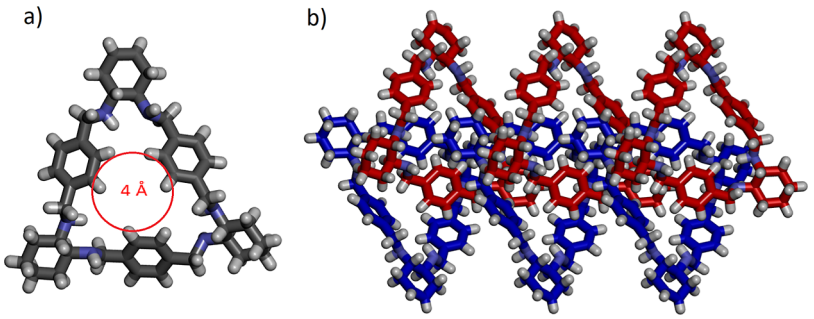

Figure 1. (a) Trianglamine macrocycle **Δ** with a 4 Å inner diameter (N, blue; C, gray; H, white) and (b) crystal packing in stick representation.

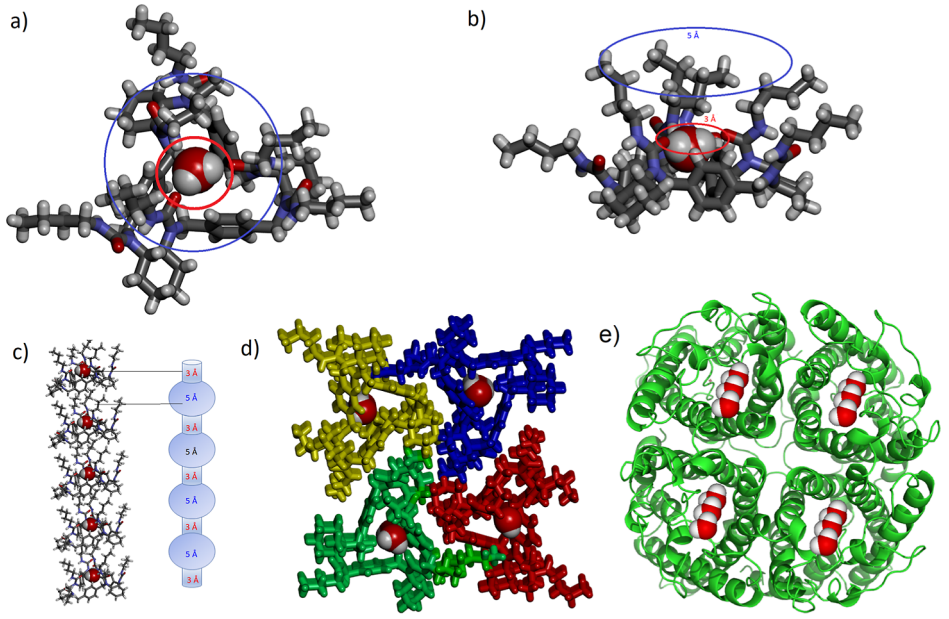

Figure 2. (a) Top and (b) lateral view of crystal structures in stick representation of (±)**ΔC4** encapsulating a water molecule inside a 3 Å triamide H-bonding pocket (N, blue; C, gray; O, red; H, white). (c) Lateral view channel type packing of (±)**ΔC4** composed of external hydrophobic platform (blue) of 5 Å diameter and of narrowest twisted triamide pore (red) of 3 Å diameter encapsulating water in CPK representation. (d) Tetrameric crystal packing of alkyl-ureido-trianglamine channels, reminiscent with (e) tetrameric protein structure of human AQP1 (Reproduced with permission from ref 48. Copyright 2001, Springer Nature).

(±)**ΔC12** become sharper and the proton resonances could be assigned as a mixture of diastereoisomers of trianglamines, as previously assigned for(±)**Δ**. The ^{13}C NMR (Figures S26–S29), ESI mass spectra, and high-resolution elemental analysis confirmed the successful functionalization with correct molecular weights for hexasubstituted compounds (±)**ΔC4**, (±)**ΔC6**, (±)**ΔC8**, and (±)**ΔC12** (Figures S30–S37). Their structures were further supported by ATR-FTIR spectra where new intense bands at ν_{N-C} = 1540 cm^{-1} and $\nu_{C=O}$ = 1620 cm^{-1} and ν_{CH2as} = 2852 cm^{-1} and ν_{CH2sim} = 2925 cm^{-1} assigned to the stretching vibrations of urea bonds and methylene moieties of alkyl chains appeared (Figures S38–S39). TGA analysis shows that the self-assembled alkyl-urea-trianglamines decomposed at higher temperature 400 °C compared to that at 350–400 °C for the unfunctionalized trianglamine (Figure S40).

Self-Aggregation in Solution. To gain insight into the mechanism of formation of AWC aggregates via self-assembly, we monitored, by dynamic light scattering (DLS) experiments, **Δ** and **ΔCX** samples that were dissolved in an ethanol, followed by sonication. The aggregation behaviors were strongly dependent on the concentration of (±)**Δ**, (±)**ΔCX**, and the solvent (EtOH)/nonsolvent (H_2O) volume ratios. Herein, for 0.5 and 0.9 wt % solutions of **Δ**, (±)**ΔCX**, a linear increase of the hydrodynamic diameter D_h of colloidal aggregates was observed after adding a certain amount of water, from D_h = 400 to D_h = 1200 nm for (±)**Δ**, (±)**ΔC4** and from D_h = 500 to D_h = 2000 nm for the more lipophilic ones (±)**ΔC6** and (±)**ΔC8** (Figure S41), without any visible precipitation. The constant increase of the dimension of D_h particles shows an increased aggregation behavior for longer alkyl tails such as (±)**ΔC12** for which the aggregation was very fast in comparison, the trianglamine (±)**Δ** where smaller layered particles are observed.

X-Ray Single-Crystal Structure. In order to have more precise information about possible molecular packing and their self-assembly behaviors, compounds ± **Δ** and (±)**ΔC4** were crystallized by slow evaporation (3 days) of solvents from ethyl acetate/benzene mixtures, resulting in the formation of good quality crystals useful for X-ray structure determination (Figure 1). The single structures of (±)**Δ**.**HCl** have previously been reported (Figure S42).[40] The single-crystal X-ray structures of (±)**Δ** (Figure 1a) confirm the macrocyclic trianglamine superstructure in which the central phenyl rings are slightly

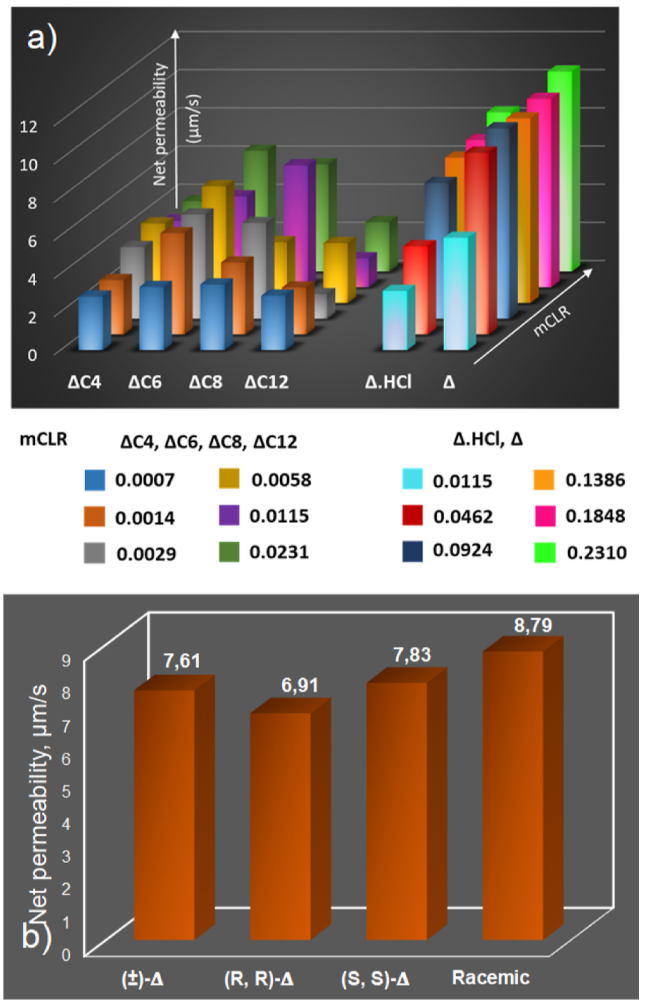

Figure 3. Water transport activity in liposomes through **Δ**-channels. Comparison of net permeability values for (a) Δ-channels at different mCLRs and for (b) commercial diasteroisomeric(±)**Δ**, enantiomeric $(R,R)_3$**Δ** and $(S,S)_3$**Δ**, and their racemic mixture (MCLR = 0.231) determined by stopped-flow light scattering experiments under hypertonic conditions abruptly exposed to a solution of 200 mM D(+)-sucrose as osmolyte (Δ_{osm} = 212 mOsm/kg).

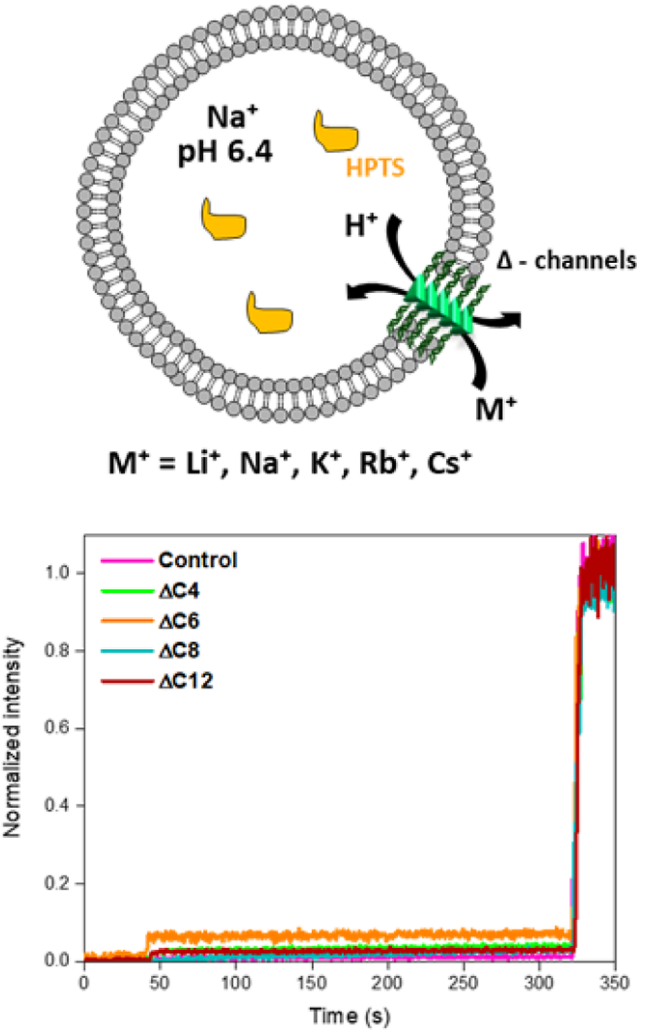

Figure 4. Comparison of Na^+ transport activity expressed as normalized fluorescence intensity of 1 mM Δ-alkyl channels containing in the extravesicular media 100 mM NaCl in PBS (pH 6.4) together with a schematic representation of the M^+/H^+ antiport mechanism that should occur through the assembled channels.

twisted, closing a free water hydrophobic pore of 4 Å diameter (Figure 1). It consists of the selective crystallization of a mixture of $(R,R)_3$**Δ** and $(S,S)_3$**Δ** to form a single crystal of (±)**Δ**. This suggests a possibility that the solubility in solvents is different among the diastereomers and that the specific diastereomers $(R,R)_3$**Δ** and $(S,S)_3$**Δ** tend to form a possible self-assembled structure in the lipid bilayers. In the crystal, each macrocycle interacts with two neighboring ones so cyclohexyl and phenyl groups fill the interstices so that all available void space between the components is filled. Accordingly, arrays of closed packed trianglamines are generated in the solid state. The alternative packing (±) **Δ** single-crystal structure is different from previously reported (R,R)**Δ** single-crystal tubular packing which is strongly dependent on the used crystallization solvent.[46,47]

The single-crystal X-ray structures of (±)**ΔC4** confirm the selective crystallization of a mixture of $(R,R)_3$**ΔC4** and $(S,S)_3$**ΔC4** (Figure 2) and confirm the coupling of six alkyl-ureido groups to the trianglamine backbone, resulting in the formation of a "bouquet"-molecule conformation. Three amide groups of lateral alkyl-urea chains display two donor N−H and one acceptor C═O groups optimally fitting the space to form anchoring H-bonds around one water molecule. Importantly a single water molecule is strongly encapsulated in the pocket jointly formed by the lateral arms (Figure 2a,b), which induce the constriction of the triangular backbone of the central phenyl segment toward the narrowest twisted water binding pores of 3 Å diameter, superposed with larger hydrophobic pockets of 5 Å diameter between the macrocycles (Figure 2c).

The other three lateral arms adaptively bind to neighboring arms bridging different trianglamines to form a network of four water channels in the solid state via hydrophobic packing of cyclohexane rings of monomers in the center of the tetramer (Figure 2d), reminiscent with human AQP1 tetrameric structure (Figure 2e).[4] This amazing biomimetic directional pore offers a combined size restriction of 3 Å H-bonding pore and a large hydrophobic pocket of 5 Å reminiscent to natural AQPs that selectively allows water molecules for a fast transit of the overall structure and together with a selective rejection of the hydrated cations. Finally, this structure does not allow any water wire formation in the solid state that could be an

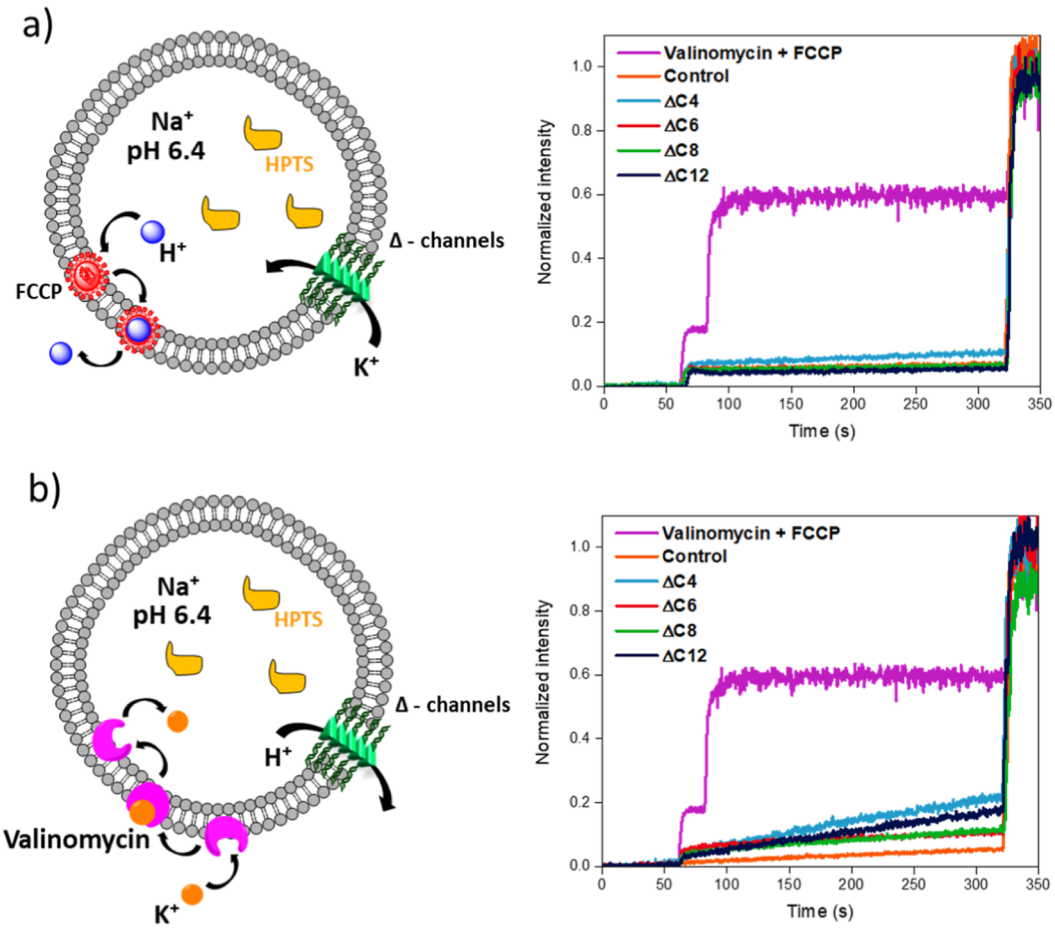

Figure 5. Coupled transport experiments of (±)**ΔCX** channels (1 mM) with (a) FCCP (50 μM) as H^+ carrier and (b) valinomycin K^+ carrier (50 μm) and containing 100 mM KCl in PBS (pH 6.4) in the extravesicular media.

important premise for proton rejection as observed for AQPs.[5,6]

Liposome Transport Experiments. In order to check the transport performances of the trianglamine channels, the compounds (±)**Δ**, $(R,R)_3$**Δ** and $(S,S)_3$**Δ**, (±)**Δ.HCl**, (±)**ΔC4**, (±)**ΔC6**, and (±)**ΔC8** were tested for water, ion, and proton transport. The water transport experiments were assessed by standard stopped-flow technique.[12] The method is based on mixing two osmolyte D(+)-sucrose solutions of different concentrations; thus, the instrument detects the shrinkage rate of vesicles under osmotic pressure determined by the induced outward water permeability through the trianglamine channels. The ion transport was conducted for different cations (Li^+, Na^+, K^+, Rb^+ and Cs^+) and was assessed by using a pH-sensitive HPTS fluorescence assay.[49] Moreover, the use of the FCCP and valinomycin as assisting H^+ and K^+ carriers, respectively, determines the intrinsic selectivity of the channels based on deconvoluted transport rates.

Water Transport Experiments. The trianglamine channels were reconstituted into a phosphatidylcholine (PC)/phosphatidylserine (PS)/cholesterol (Chl) (PC/PS/Chl) mixture with a molar ratio of 4/5/1 obtaining lipid vesicles with a 100 mm in diameter. The trianglamines (±)**Δ**, $(R,R)_3$**Δ** and $(S,S)_3$**Δ**, (±)**Δ.HCl**, (±)**ΔC4**, (±)**ΔC6**, (±)**ΔC8**, and (±)**ΔC12** were added from their DMSO solutions to the preformed vesicle suspension at different molar compound to lipid ratios (mCLRs) (see Supporting Information for details). The water transport measurements were performed under hypertonic conditions driven by an outwardly 10 mM PBS solution (pH = 6.4) of 200 mM D(+)-sucrose osmolyte. The shrinkage of the liposomes produced an increase of the light-scattering signal (Figure S49). In order to facilitate the description of the influence of the chemical structure of the trianglamine correlated with their water transport performances, the compounds were grouped in two categories, as they presented different behaviors. For the first category containing macrocyclic (±)**Δ**, (R,R)**Δ** and (S,S)**Δ**, and (±)**Δ.HCl**, the water transport rates were dependent on the concentration used of the channels; the net permeabilities show a continual increase showing a saturation behavior when mCLRs increase (Figure 3). The range of the permeabilities obtained with **Δ.HCl** and (±)**Δ**, $(R,R)_3$**Δ**, and $(S,S)_3$**Δ** is from 6.91 to 10.5 μm/s at high mCLR = 0.231 (Figure S50).

Interestingly, the net permeabilities of racemic (±)**Δ** and enantiopure $(R,R)_3$**Δ** and $(S,S)_3$**Δ** trianglamines as well as a equimolar mixture of enantiomers at a channel-to-lipid weight ratio of 0.2309 (CLR = 0.2309) are almost the same order of magnitude around 8 μm/s (Figure 3b). This observation suggests that the lipids do not exert a conformational preference, stabilizing the chiral superstructures over the racemic superstructures for which the insertion and the water transport activity do not depend on the chirality. Therefore, we pursued our studies on hydrophobic less expensive compounds (±)**ΔC4**, (±)**ΔC6**, (±)**ΔC8**, and (±)**ΔC12**.

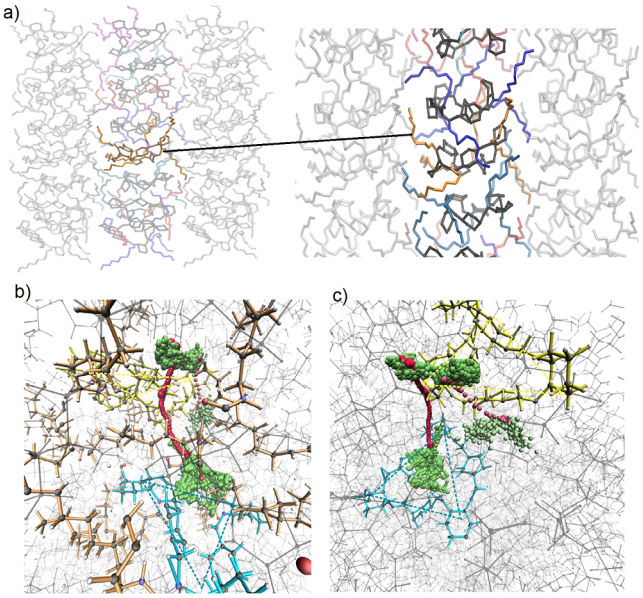

Figure 6. (a) Lateral view of the (±)**ΔC4** water channel, where 8 layers stacking after 50 ps of simulation at 300 K are shown in different snapshots obtained simulating a periodic channel structure. Snapshots (b) side view and (c) top view of a water molecule trajectory in (±)**ΔC4** channels obtained by *NPT* simulation at room temperature and ambient pressure. Two successive Δ platforms are represented in cyan and yellow. Each green or red sphere represents a position in time of the same single water molecule center of mass (over a trajectory of 25 ns). Green represents the instants in which the water molecule is H-bonded via amide bonds, while diffusion is limited, red represents instants of diffusion between layers occurring in the external pocket of the Δ in-between the alkyl arms.

When considering the second category of hydrophobic alkyl-urea-trianglamines (±)**ΔC4**, (±)**ΔC6**, (±)**ΔC8**, and (±)**ΔC12**, the water transport rates are strongly dependent on the variations of the length of the alkyl chain. (±)**ΔC4** and (±)**ΔC12** presented lower water permeabilities regardless of the concentrations used; thus, it can be stated that a more compact packing into the membrane may interfere with the water transport rates. Shorter alkyl chains provide less insertion of (±)**ΔC4** within membrane, while sterical impediments of longer chains lead to a dysfunctional insertion of (±)**ΔC12** into the membrane. The net permeabilities for (±)**ΔC4** and (±)**ΔC12** are almost the same: 2.45 to 2.85 μm/s at mCLR = 0.0014 and 2.58 to 3.68 μm/s at high mCLR = 0.0231 (Figure S40), respectively. The (±)**ΔC6** and (±)**ΔC8** trianglamines presented higher water permeabilities. For (±)**ΔC6**, the net permeability is almost constant over lower or higher mCLR (5.30 μm/s at mCLR = 0.0014 and 6.32 μm at mCLR = 0.0231). For the (±)**ΔC8** at low mCLR = 0.007−0.0014, the net permeabilities are ∼3.4−3.7 μm/s, then we observed a saturation behavior reached at mCLR = 0.0115 with a maximal net permeability of 6.38 μm/s (Figure S49).

We further estimated the single-channel permeability (P_s) of the trianglamine channels, based on their total insertion, lipid concentration, and the channel self-assembly into the lipid bilayers.

To be able to determine the single-channel permeabilities, we considered that the number of stacked molecules needed to form a channel that crosses the entire length of 35 Å of the bilayer is equal to 5 molecules, equal to the number of molecules found in the single-crystal structure of (±)**ΔC4** (Figure 2c). The single-channel permeability values varied from 2.0×10^7 water molecules/s/channel at mCLR = 0.19 for (±)**Δ** and (±)**Δ.HCl** (Table S1), while single-channel permeability values between 4×10^8 at 10 times more diluted mCLR = 0.029 were determined for lipophilic (±)**ΔC4**, (±)**ΔC8**, (±)**ΔC6**, and (±)**ΔC12** (Table S2), which are 1 or 2 orders of magnitude lower than those of AQPs (∼10^9 water molecules/s/channel).[6] **Δ** and **Δ.HCl** showed higher water net transport permeabilities for 10 times more concentration in the bilayer membranes, when compared with more lipophilic (±)**ΔC4**, (±)**ΔC6**, (±)**ΔC8**, and (±)**ΔC12**. These higher net permeabilities are reminiscent of the increased solubility of (±)**Δ** and (±)**Δ.HCl** in the membrane. The lipophilic (±)**ΔCX** generates stabilized percolated channels with higher single channel permeability, but they are less soluble in the membrane due to their aggregation. The single channel permeability is strongly enhanced for the compounds presenting higher hydrophobicity, as they can form stable cluster-type membrane aggregation that allows for fast and selective water single-channel translocation.

Cation and Proton Transport Experiments. The cation transport activity of all of the compounds was tested using the standard HPTS fluorescence assays. The large unilamellar vesicles containing PC were hydrated with a PBS buffer solution (10 mM, pH 6.4) containing an alkaline salt (LiCl, NaCl, KCl, RbCl, and CsCl) with a concentration of 100 mM. Cation (M^+ = Li^+, Na^+, K^+, Rb^+, and Cs^+) transport activities across the bilayer membrane incorporating (±)**ΔC4**, (±)**ΔC6**, (±)**ΔC8**, and (±)**ΔC12** channels were tested at the same mCLRs used for water transport (see Supporting Information for details). When tested with MCl on external buffer (±)**ΔC4**, (±)**ΔC6**, (±)**ΔC8**, and (±)**ΔC12** do not present a dose−response-type activity, showing constant nearly zero transport activity demeanor, regardless of the concentration used. **Δ.HCl** and **Δ** showed a slight change in the fluorescence intensity when base was added into the extravesicular media reminiscent of HPTS deprotonation and a rapid proton transport via the −NH groups of trianglamines. However, after the equilibrium was reached, the dose−response profile displays constant absorbance behaviors (Figures S51−S55). It is clear that M^+/H^+ antiport conductance of the trianglamine channel states across the lipid bilayer membrane is not observed for any of the studied concentrations (Figure 4).

To complement these results and check whether H^+ transport occurs through the assembled channels, the compounds were tested for K^+/H^+ antiport activity. We conducted standard HPTS assays with (±)**ΔC4**, (±)**ΔC6**, (±)**ΔC8**, and (±)**ΔC12** in the presence of cyanide 4-(trifluoromethoxy)phenylhydrazone (FCCP) as a H^+ carrier and valinomycin as a K^+ carrier (Figure S56).

The membrane polarization via FCCP and valinomycin for (±)**ΔC4**, (±)**ΔC6**, (±)**ΔC8**, and (±)**ΔC12** does not generate an increase in fluorescence intensity, meaning that their channel structuration is not suitable to accommodate K^+/H^+ antiport (Figure 5). In the case of (±)**Δ** and (±)**Δ.HCl**, it generated a strong initial increase in fluorescence intensity, but after pH equilibrium was reached, the dose−response experiments had a constant absorbance acquisition. Overall, all tested compounds had very low total inactivity for K^+ and H^+ transport in the presence of FCCP and valinomycin.

Molecular Dynamic Simulations. Molecular dynamics simulations (see Supporting Information for details) have been used to test the stability of self-assembled superstructures

formed by stackings of eight (±)**ΔC4** macrocycles as extracted from its crystal structure of eight bundles of a mixture of $(R,R)_3$**ΔC4** and $(S,S)_3$**ΔC4** and immersed in water at room temperature. We noted that the stabilization effect of the stackings by the alkyl chains via H-bonding and hydrophobic effects prevents exfoliation of the layers (Figure 6). This confirms that it is thermodynamically possible to obtain stable regular self-assembled channels as observed experimentally. The monomer highlighted in orange, while other monomers have a semitransparent shading in order to increase visual contrast in Figure 6a, has three lateral ureido-alkyl arms pointing up and the other three pointing down.

The ureido-alkyl arms appear to interpenetrate with each other, creating a locking mechanism of these monomers that stabilizes the overall structure. This highlights the importance of the interplay between the different monomers and their alkyl arms in creating a functional and stable trianglamine channel.

The (±)**ΔC4** stackings that contain eight layers have a length of approximately 50 Å; as a result, the interlayer distance is 6 Å, which is in agreement with the experimental expectations of having 5 molecules stacking to form a 35 Å channel. The narrowest pore size, perpendicular to the channel length, is 3 Å in accordance with the obtained X-ray results. Thus, the channel can accommodate water molecules with a kinetic diameter of 2.65 Å. Further molecular simulations allowed us to assess whether the water-charged superstructures may selectively accommodate water translocation. These simulation results taken together suggest that at some stage, the lateral amide arms may rearrange so water is oscillating into a sponge like form (green trajectories shown in Figure 6b,c), to give rise to a limited water flow stabilized via amide H-bonding in this narrowest region of the pore. Radial distribution function (Figure S57) between water molecules and the channel shows a peak at a distance of 1.8 Å, suggesting that strong H-bonding between water molecules is occurring within the channel. With such a stabilized water cluster, water transport is indeed observed between different clusters and it is occurring in the external hydrophobic pocket of the Δ platforms in-between the alkyl arms (red trajectories shown in Figure 6b,c). The distribution of restrictive pore sizes along a variable porous structure reflects the transient appearance of water clusters between these regions inside the channel. For such narrow pores, the entrance of hydrated ions into the channels is restricted by the dehydration energy penalty arising from their incomplete hydration within (±)**ΔC4** channels. The water cluster stabilization via H-bonding to amide bonds confers to these channels selective behaviors that make the intrinsic features of small pores particularly self-protective against ions.

We show that systematic functionalization of trianglamine macrocycles with alkyl-ureido chains leads to highly effective and selective AWCs. Simple use of such lateral amide arms led to the formation of an unexpected binding/recognition of one water molecule within a selective pocket of the molecular receptor via a combination of three donor−acceptor H-bonds of lateral amide arms. It results in an increased water-transport activity at lower concentration of the alkyl-ureido-trianglamine channels within membranes. The stacking of several trianglamines led to the formation of such pocket-decorated pores conferring selective binding for water accompanied by the formation of larger pores between trianglamines favorable for fast water translocation.

From a mechanistic point of view, the H-bonding network offered by the six-armed alkyl-ureido arms can act itself as a recognition-based barrier with high selectivity for water translocation. Moreover, the H-bonding of water molecules can intervene with both donor and acceptor H-bonds, satisfying the full number of hydrogen bonds within the pocket and making possible its facilitated translocation through the gate. Oppositely, the energy penalty for binding either cations or anions would be too high, as the entrance of hydrated ions into the channels may be restricted by the dehydration energy penalty arising from the preference of ions to be surrounded by water molecules rather than incomplete hydration within trianglamine channels. The distribution of pockets along the channel is not continual and reflects a transient appearance of single water molecules inside the channel, so proton translocation through such discontinuous waters is prohibited. It is very tempting to equate that selective water binding pockets can form permeable waters in the bilayer membrane, so that triangle channels feature this rather unique selective permeability of water, rejecting ions and protons.

CONCLUSIONS

In summary, we have developed a new class of AWCs based on self-assembled trianglamines and alkyl-ureido trianglamines. They self-assembled in directional channels that present enhanced selective water permeability with almost total proton rejection across a lipid bilayer. More importantly, the structuration of these channels is not suitable to accommodate hydrated cations and presents total salt rejection, which can offer a close approach in mimicking the functions of natural AQPs. The results presented here are of great importance, as these AWCs showed adaptive behaviors of water inside the channels being strongly dependent on the dimension and structuration of the channels and being active at the very low concentration used. The trianglamine channels described here, which are capable of mimicking the natural functions of AOPs, are holding significant promise for further developing energy-effective membranes for water desalination.

Corresponding Authors

Mona Semsarilar − *Institut Européen des Membranes (IEM), Univ Montpellier, CNRS, ENSCM, Montpellier 34090,*

France; orcid.org/0000-0002-1544-1824; Email: Mona.semsarilar@umontpellier.fr

Mihail Barboiu − *Institut Européen des Membranes (IEM), Univ Montpellier, CNRS, ENSCM, Montpellier 34090, France*; orcid.org/0000-0003-0042-9483; Email: mihail-dumitru.barboiu@umontpellier.fr

Authors

Iuliana M. Andrei − *Institut Européen des Membranes (IEM), Univ Montpellier, CNRS, ENSCM, Montpellier 34090, France*

Arnaud Chaix − *Institut Européen des Membranes (IEM), Univ Montpellier, CNRS, ENSCM, Montpellier 34090, France*

Belkacem Tarek Benkhaled − *Institut Européen des Membranes (IEM), Univ Montpellier, CNRS, ENSCM, Montpellier 34090, France*

Romain Dupuis − *Laboratoire de Mécanique et Génie Civil (LMGC), University of Montpellier, CNRS—UMR 5508, Montpellier 34090, France*; orcid.org/0000-0001-9451-1132

Chaimaa Gomri − *Institut Européen des Membranes (IEM), Univ Montpellier, CNRS, ENSCM, Montpellier 34090, France*

Eddy Petit − *Institut Européen des Membranes (IEM), Univ Montpellier, CNRS, ENSCM, Montpellier 34090, France*

Maurizio Polentarutti − *Elettra-Sincrotrone Trieste S.C.p.A., Basovizza 34149 Trieste, Italy*

Arie van der Lee − *Institut Européen des Membranes (IEM), Univ Montpellier, CNRS, ENSCM, Montpellier 34090, France*; orcid.org/0000-0002-4567-1831

Complete contact information is available at: https://pubs.acs.org/10.1021/jacs.3c02815

Author Contributions

‖I.M.A. and A.C. contributed equally to this work.

Notes

The authors declare no competing financial interest.

■ ACKNOWLEDGMENTS

This project has received funding from the European Union's Horizon 2020 research and innovation programme under the Marie Skłodowska-Curie grant agreement no. 860592. The authors would also like to thank the French National Research Agency (ANR) and MUSE (University of Montpellier) for funding the postdoctoral positions of T.B. (PEPPISA-19-CE06-0011-01) and A.C. (Soutien à la recherche-IMOPS).

■ REFERENCES

(1) Mekonnen, M. M.; Hoekstra, A. Y. Sustainability: Four Billion People Facing Severe Water Scarcity. *Sci. Adv.* **2016**, *2*, No. e1500323.

(2) Boretti, A.; Rosa, L. Reassessing the Projections of the World Water Development Report. *npj Clean Water* **2019**, *2*, 15.

(3) Tajkhorshid, E.; Nollert, P.; Jensen, M.; Miercke, L. J. W.; O'Connell, J.; Stroud, R. M.; Schulten, K. Control of the Selectivity of the Aquaporin Water Channel Family by Global Orientational Tuning. *Science* **2002**, *296*, 525−530.

(4) Carrillo, D. R.; Ying, J. T. Y.; Darwis, D.; Soon, C. H.; Cornvik, T.; Torres, J.; Lescar, J. Crystallization and preliminary crystallographic analysis of human aquaporin 1 at a resolution of 3.28 angstrom. *Acta Crystallogr., Sect. F: Struct. Biol. Commun.* **2014**, *70*, 1657−1663.

(5) Kosinska Eriksson, U.; Fischer, G.; Friemann, R.; Enkavi, G.; Tajkhorshid, E.; Neutze, R. Subangstrom Resolution X-Ray Structure Details Aquaporin-Water Interactions. *Science* **2013**, *340*, 1346−1349.

(6) Agre, P. Aquaporin Water Channels (Nobel Lecture). *Angew. Chem., Int. Ed.* **2004**, *43*, 4278−4290.

(7) Shen, Y. x.; Saboe, P. O.; Sines, I. T.; Erbakan, M.; Kumar, M. Biomimetic Membranes: A Review. *J. Membr. Sci.* **2014**, *454*, 359−381.

(8) Hélix-Nielsen, C. Biomimetic Membranes as a Technology Platform: Challenges and Opportunities. *Membranes* **2018**, *8*, 44.

(9) Le Duc, Y.; Michau, M.; Gilles, A.; Gence, V.; Legrand, Y. M.; van der Lee, A.; Tingry, S.; Barboiu, M. Imidazole-Quartet Water and Proton Dipolar Channels. *Angew. Chem., Int. Ed.* **2011**, *50*, 11366−11372.

(10) Shen, Y. X.; Song, W. C.; Barden, D. R.; Ren, T.; Lang, C.; Feroz, H.; Henderson, C. B.; Saboe, P. O.; Tsai, D.; Yan, H.; Butler, P. J.; Bazan, G. C.; Phillip, W. A.; Hickey, R. J.; Cremer, P. S.; Vashisth, H.; Kumar, M. Achieving High Permeability and Enhanced Selectivity for Angstrom-Scale Separations Using Artificial Water Channel Membranes. *Nat. Commun.* **2018**, *9*, 2294.

(11) Huang, L. B.; Hardiagon, A.; Kocsis, I.; Jegu, C. A.; Deleanu, M.; Gilles, A.; Van Der Lee, A.; Sterpone, F.; Baaden, M.; Barboiu, M. Hydroxy Channels-Adaptive Pathways for Selective Water Cluster Permeation. *J. Am. Chem. Soc.* **2021**, *143*, 4224−4233.

(12) Licsandru, E.; Kocsis, I.; Shen, Y. X.; Murail, S.; Legrand, Y. M.; Van Der Lee, A.; Tsai, D.; Baaden, M.; Kumar, M.; Barboiu, M. Salt-Excluding Artificial Water Channels Exhibiting Enhanced Dipolar Water and Proton Translocation. *J. Am. Chem. Soc.* **2016**, *138*, 5403−5409.

(13) Murail, S.; Vasiliu, T.; Neamtu, A.; Barboiu, M.; Sterpone, F.; Baaden, M. Water Permeation across Artificial I-Quartet Membrane Channels: From Structure to Disorder. *Faraday Discuss.* **2018**, *209*, 125−148.

(14) Huang, L. B.; Di Vincenzo, M.; Ahunbay, M. G.; Van Der Lee, A.; Cot, D.; Cerneaux, S.; Maurin, G.; Barboiu, M. Bilayer versus Polymeric Artificial Water Channel Membranes: Structural Determinants for Enhanced Filtration Performances. *J. Am. Chem. Soc.* **2021**, *143*, 14386−14393.

(15) Tunuguntla, R. H.; Henley, R. Y.; Yao, Y. C.; Pham, T. A.; Wanunu, M.; Noy, A. Enhanced Water Permeability and Tunable Ion Selectivity in Subnanometer Carbon Nanotube Porins. *Science* **2017**, *357*, 792−796.

(16) Shen, J.; Ye, R.; Romanies, A.; Roy, A.; Chen, F.; Ren, C.; Liu, Z.; Zeng, H. Aquafoldmer-Based Aquaporin-like Synthetic Water Channel. *J. Am. Chem. Soc.* **2020**, *142*, 10050−10058.

(17) Hu, X. B.; Chen, Z.; Tang, G.; Hou, J. L.; Li, Z. T. Single-Molecular Artificial Transmembrane Water Channels. *J. Am. Chem. Soc.* **2012**, *134*, 8384−8387.

(18) Yan, Z. J.; Wang, D.; Ye, Z.; Fan, T.; Wu, G.; Deng, L.; Yang, L.; Li, B.; Liu, J.; Ma, T.; Dong, C.; Li, Z. T.; Xiao, L.; Wang, Y.; Wang, W.; Hou, J. L. Artificial Aquaporin That Restores Wound Healing of Impaired Cells. *J. Am. Chem. Soc.* **2020**, *142*, 15638−15643.

(19) Strilets, D.; Fa, S.; Hardiagon, A.; Baaden, M.; Ogoshi, T.; Barboiu, M. Biomimetic Approach for Highly Selective Artificial Water Channels Based on Tubular Pillar[5]Arene Dimers. *Angew. Chem., Int. Ed.* **2020**, *59*, 23213−23219.

(20) Chen, L.; Si, W.; Zhang, L.; Tang, G.; Li, Z. T.; Hou, J. L. Chiral Selective Transmembrane Transport of Amino Acids through Artificial Channels. *J. Am. Chem. Soc.* **2013**, *135*, 2152−2155.

(21) Song, W.; Joshi, H.; Chowdhury, R.; Najem, J. S.; Shen, Y. x.; Lang, C.; Henderson, C. B.; Tu, Y. M.; Farell, M.; Pitz, M. E.; Maranas, C. D.; Cremer, P. S.; Hickey, R. J.; Sarles, S. A.; Hou, J. l.; Aksimentiev, A.; Kumar, M. Artificial Water Channels Enable Fast and Selective Water Permeation through Water-Wire Networks. *Nat. Nanotechnol.* **2020**, *15*, 73−79.

(22) Yuan, Y. D.; Dong, J.; Liu, J.; Zhao, D.; Wu, H.; Zhou, W.; Gan, H. X.; Tong, Y. W.; Jiang, J.; Zhao, D. Porous Organic Cages as Synthetic Water Channels. *Nat. Commun.* **2020**, *11*, 4927.

(23) Mondal, D.; Dandekar, B. R.; Ahmad, M.; Mondal, A.; Mondal, J.; Talukdar, P. Selective and rapid water transportation across a self-assembled peptide-diol channel via the formation of a dual water array. *Chem. Sci.* **2022**, *13*, 9614−9623.
(24) Itoh, Y.; Chen, S.; Hirahara, R.; Konda, T.; Aoki, T.; Ueda, T.; Shimada, I.; Cannon, J. J.; Shao, C.; Shiomi, J.; Tabata, K. V.; Noji, H.; Sato, K.; Aida, T. Ultrafast water permeation through nanochannels with a densely fluorous interior surface. *Science* **2022**, *376*, 738−743.
(25) Huang, L. B.; Di Vincenzo, M.; Li, Y.; Barboiu, M. Artificial Water Channels: Towards Biomimetic Membranes for Desalination. *Chem.—Eur. J.* **2021**, *27*, 2224−2239.
(26) Huang, T.; Alyami, M.; Kashab, N. M.; Nunes, S. P. Engineering Membranes with Macrocycles for Precise Molecular Separations. *J. Mater. Chem.* **2021**, *9*, 18102−18128.
(27) Pedersen, C. J. The Discovery of Crown Ethers. *Science* **1988**, *241*, 536−540.
(28) Atwood, J. L.; Koutsantonis, G. A.; Raston, C. L. Purification of C60 and C70 by Selective Complexation with Calixarenes. *Nature* **1994**, *368*, 229−231.
(29) Lee, J. W.; Samal, S.; Selvapalam, N.; Kim, H. J.; Kim, K. Cucurbituril Homologues and Derivatives: New Opportunities in Supramolecular Chemistry. *Acc. Chem. Res.* **2003**, *36*, 621−630.
(30) Ogoshi, T.; Kanai, S.; Fujinami, S.; Yamagishi, T. A.; Nakamoto, Y. Para-Bridged Symmetrical Pillar[5]Arenes: Their Lewis Acid Catalyzed Synthesis and Host-Guest Property. *J. Am. Chem. Soc.* **2008**, *130*, 5022−5023.
(31) Kaik, M.; Gawroński, J. Unprecedented Selectivity in the Formation of Large-Ring Oligoimines from Conformationally Bistable Chiral Diamines. *Org. Lett.* **2006**, *8*, 2921−2924.
(32) Dawn, S.; Dewal, M. B.; Sobransingh, D.; Paderes, M. C.; Wibowo, A. C.; Smith, M. D.; Krause, J. A.; Pellechia, P. J.; Shimizu, L. S. Self-Assembled Phenylethynylene Bis-Urea Macrocycles Facilitate the Selective Photodimerization of Coumarin. *J. Am. Chem. Soc.* **2011**, *133*, 7025−7032.
(33) Nalluri, S. K. M.; Liu, Z.; Wu, Y.; Hermann, K. R.; Samanta, A.; Kim, D. J.; Krzyaniak, M. D.; Wasielewski, M. R.; Stoddart, J. F. Chiral Redox-Active Isosceles Triangles. *J. Am. Chem. Soc.* **2016**, *138*, 5968−5977.
(34) Neira, I.; Blanco-Gómez, A.; Quintela, J. M.; García, M. D.; Peinador, C. Dissecting the "Blue Box": Self-Assembly Strategies for the Construction of Multipurpose Polycationic Cyclophanes. *Acc. Chem. Res.* **2020**, *53*, 2336−2346.
(35) Wu, J. R.; Yang, Y. W. Synthetic Macrocycle-Based Nonporous Adaptive Crystals for Molecular Separation. *Angew. Chem., Int. Ed.* **2021**, *60*, 1690−1701.
(36) Jie, K.; Zhou, Y.; Li, E.; Li, Z.; Zhao, R.; Huang, F. Reversible Iodine Capture by Nonporous Pillar[6]Arene Crystals. *J. Am. Chem. Soc.* **2017**, *139*, 15320−15323.
(37) Patil, R. S.; Kumari, H.; Barnes, C. L.; Atwood, J. L. Engineering Supramolecular Organic Frameworks (SOFs) of C-Alkylpyrogallol[4]Arene with Bipyridine-Based Spacers. *Chem. Commun.* **2015**, *51*, 2304−2307.
(38) Patil, R. S.; Zhang, C.; Barnes, C. L.; Atwood, J. L. Construction of Supramolecular Organic Frameworks Based on Noria and Bipyridine Type Spacers. *Cryst. Growth Des.* **2017**, *17*, 7−10.
(39) Luo, X. Z.; Jia, X. J.; Deng, J. H.; Zhong, J. L.; Liu, H. J.; Wang, K. J.; Zhong, D. C. A Microporous Hydrogen-Bonded Organic Framework: Exceptional Stability and Highly Selective Adsorption of Gas and Liquid. *J. Am. Chem. Soc.* **2013**, *135*, 11684−11687.
(40) Chaix, A.; Mouchaham, G.; Shkurenko, A.; Hoang, P.; Moosa, B.; Bhatt, P. M.; Adil, K.; Salama, K. N.; Eddaoudi, M.; Khashab, N. M. Trianglamine-Based Supramolecular Organic Framework with Permanent Intrinsic Porosity and Tunable Selectivity. *J. Am. Chem. Soc.* **2018**, *140*, 14571−14575.
(41) Chappanda, K. N.; Chaix, A.; Surya, S. G.; Moosa, B. A.; Khashab, N. M.; Salama, K. N. Trianglamine Hydrochloride Crystals for a Highly Sensitive and Selective Humidity Sensor. *Sens. Actuators, B* **2019**, *294*, 40−47.
(42) Huang, T.; Moosa, B. A.; Hoang, P.; Liu, J.; Chisca, S.; Zhang, G.; AlYami, M.; Khashab, N. M.; Nunes, S. P. Molecularly-Porous Ultrathin Membranes for Highly Selective Organic Solvent Nanofiltration. *Nat. Commun.* **2020**, *11*, 5882.
(43) Dey, A.; Chand, S.; Maity, B.; Bhatt, P. M.; Ghosh, M.; Cavallo, L.; Eddaoudi, M.; Khashab, N. M. Adsorptive Molecular Sieving of Styrene over Ethylbenzene by Trianglimine Crystals. *J. Am. Chem. Soc.* **2021**, *143*, 4090−4094.
(44) Dey, A.; Chand, S.; Ghosh, M.; Altamimy, M.; Maity, B.; Bhatt, P. M.; Bhat, I. A.; Cavallo, L.; Eddaoudi, M.; Khashab, N. M. Molecular Recognition and Adsorptive Separation Ofm-Xylene by Trianglimine Crystals. *Chem. Commun.* **2021**, *57*, 9124−9127.
(45) Hua, B.; Ding, Y.; Alimi, L. O.; Moosa, B.; Zhang, G.; Baslyman, W. S.; Sessler, J.; Khashab, N. M. Tuning the Porosity of Triangular Supramolecular Adsorbents for Superior Haloalkane Isomer Separations. *Chem. Sci.* **2021**, *12*, 12286−12291.
(46) Gawronski, J.; Gawronska, K.; Grajewski, J.; Kwit, M.; Plutecka, A.; Rychlewska, U. Trianglamines - Readily Prepared, Conformationally Flexible Inclusion-Forming Chiral Hexamines. *Chem.—Eur. J.* **2006**, *12*, 1807−1817.
(47) Chadim, M.; Buděšínský, M.; Hodacova, J.; Závada, J.; Junk, P. C. (3 + 3)-Cyclocondensation of the enantiopure and racemic forms of trans-1,2-diaminocyclohexane with terephthaldehyde. Formation of diastereomeric molecular triangles and their stereoselective solid-state stacking into microporous chiral columns. *Tetrahedron: Asymmetry* **2001**, *12*, 127−133.
(48) Sui, H.; Han, B. G.; Lee, J. K.; Walian, P.; Jap, B. K. Structural Basis of Water-Specific Transport through the AQP1 Water Channel. *Nature* **2001**, *414*, 872−878.
(49) Matile, S.; Sakai, N.; Hennig, A. Transport Experiments in Membranes Gale, P. A., Steed, J. W., Eds.; Wiley: Chichester, U.K., 2012; Vol. 2, pp 473−500.*Supramolecular Chemistry: From Molecules to Nanomaterials*